

Computed Local Chemical Reactivity of Melanoidins Red M1 and Red M2 Using Conceptual DFT

Juan Frau¹ and Daniel Glossman-Mitnik^{1,2*}

DOI: 10.25177/JCCMM.3.1.RA.460

Research

Received Date: 25th Jan 2019Accepted Date: 11th Feb 2019Published Date: 17th Feb 2019

Copy rights: © This is an Open access article distributed under the terms of International License.



¹Departament de Química, Universitat de les Illes Balears, Carretera a Valldemossa, Km 7.5, 07122 Palma de Mallorca, Spain.

²Laboratorio Virtual NANOCOSMOS, Departamento de Medio Ambiente y Energía, Centro de Investigación en Materiales Avanzados, Miguel de Cervantes 120, Complejo Industrial Chihuahua, Chih 31136 Chihuahua, Mexico.

CORRESPONDENCE AUTHOR

Daniel Glossman-Mitnik,
Email: daniel.glossman@cimav.edu.mx

CITATION

Daniel Glossman-Mitnik et al., Computed Local Chemical Reactivity of Melanoidins Red M1 and Red M2 Using Conceptual DFT(2019) SDRP Journal of Computational Chemistry & Molecular Modelling 3(1) p:235-251

ABSTRACT

This study assessed ten density functionals, including CAM-B3LYP, LC- ω PBE, M11, M11L, MN12L, MN12SX, N12, N12SX, ω B97X, and ω B97XD related to the Def2TZVP basis set together with the SMD solvation model in the calculation of the molecular properties and structures of the Red-M1 and Red-M2 intermediate melanoidin pigments. The global and local chemical reactivity descriptors for the systems were calculated via the Conceptual Density Functional Theory. The choice of the active sites applicable to nucleophilic, electrophilic as well as radical attacks was made by linking them with the Fukui function indices, the electrophilic Parr functions, and the condensed dual descriptor $\Delta f(r)$ over the atomic sites. The prediction of the maximum absorption wavelength directly from the HOMO–LUMO tended to be considerably accurate relative to the experimental values for the MN12SX and N12SX density functionals. This study found the MN12SX and N12SX density functionals to be the most appropriate to predict the chemical reactivity of the molecules under consideration.

Keywords: Melanoidins; Red-M1; Red-M2; Conceptual DFT; Chemical Reactivity; Dual Descriptor; Parr Function; Maximum Absorption Wavelength

INTRODUCTION

Melanoidins are brown pigments formed during the reaction of reducing sugars with amino groups, derived from amino acids, amines, and proteins. Their chemical structure is largely unknown, but their functional properties have been a matter of intensive study because of their abundance in heat-treated foods. Melanoidin formation contributes to the development of aroma and color in processed foods, as well as food texture and beverage viscosity [1].

Melanoidins are considered as the final products of a process known as non-enzymatic browning or the Maillard reaction. A similar reaction between reducing sugars and biological molecules takes place under physiological conditions, in a process usually called glycation. Glycation has a significant impact on the aging of living organisms and the pathology of some diseases [1]. We have recently dedicated much effort to understand the glycation process, which is mainly associated with certain diseases like Diabetes, Alzheimer, and Parkinson, as well as the chemical reactivity of the reducing carbohydrates, amino acids, and small peptides that participate in it [2–9].

Although color formation is the primary characteristic of the Maillard reaction, our knowledge of the colored moieties responsible for the coloration is still only rudimentary. The low-weight intermediate colored products are known as colored Maillard reaction products (CMRP) and the color produced can be readily measured by reading the absorbance in the visible region of the spectrum, with the typical wavelengths used being 360 and 420 nm [10].

These CMRPs are of great interest not only in the food industry, but also for their potential application as photosensitizers, as antioxidants related to health and as colorants to be used in dye-sensitized solar cells for the production of alternative energy. Thus, there is a great interest in studying their chemical properties, with special emphasis on their molecular reactivity.

Conceptual Density Functional Theory (CDFT, also known as Chemical Reactivity Theory) is a powerful

tool for the prediction, analysis, and interpretation of the outcome of chemical reactions [11–14].

Two interesting CMRPs amenable to being studied through conceptual DFT are Red-M1 and its diastereomer Red-M2 [15], which are red pigments isolated from the reaction system between D-xylose and glycine. Therefore, we believe that it could be of interest to apply the concepts of DFT to the study of the chemical reactivity of these red pigments.

In order to obtain quantitative values of the conceptual DFT descriptors, it is necessary to utilize the Kohn–Sham (KS) theory through calculations of the molecular density, the energy of the system, and the orbital energies - specifically those related to the frontier orbitals; that is, the highest occupied molecular orbital (HOMO) and lowest unoccupied molecular orbital (LUMO) [16–21].

In recent years, there has been significant interest in the use of range-separated (RS) exchange-correlation functionals in KS DFT [22]. These functionals partition the $1/r_{12}$ operator in the exchange term into short- and long-range components, with a range-separation parameter, ω , controlling the rate at which the long-range behavior is attained. The value of ω can be fixed or it can be “tuned” on a system-by-system basis by minimizing some tuning norm. The optimal tuning approach is based on the knowledge that in exact KS and generalized KS theory, the energy of the HOMO, $\varepsilon_H(N)$, for an N-electron system should be exactly $-IP(N)$, where IP is the vertical ionization potential calculated with a given functional as the energy difference $E(N-1) - E(N)$. With approximate functionals, the differences between $\varepsilon_H(N)$ and $-IP(N)$ can be very large. Optimal tuning implies a non-empirical determination of a system-specific range-separation parameter ω in an RSE functional and, optionally, other parameters, such that $\varepsilon_H(N) = -IP(N)$ is satisfied to the best possible degree [23]. Although there is no equivalency to this prescription for the electron affinity (EA), and the LUMO of the neutral species, it can be said that $\varepsilon_H(N+1) = -EA(N)$, thus making it possible to find an optimized ω value that is simultaneously optimized for getting both

properties, rendering it useful for an easy prediction of conceptual DFT descriptors. In previous works [2–9], we have termed this simultaneous prescription as the “KID procedure” for its analogy with the Koopmans’ theorem.

This means that the goodness of a given density functional for the purpose of predicting the conceptual DFT descriptors directly from the properties of the neutral molecule can be estimated by checking how well it follows the KID procedure. However, this tune optimization is system-dependent, and it must be performed for each molecule. Thus, it will be interesting to consider several recent density functionals that have shown great accuracy across a broad spectrum of databases in chemistry and physics and where the value of ω is fixed to evaluate their performance in fulfilling this practical technique.

The objective of this work is to conduct a comparative study of the performance of some recent density functionals for reproducing the chemical reactivity descriptors of the Red-M1 and Red-M2 pigments within the KID formalism to gain insight into their molecular properties that can be used for future studies on the chemical reactivity of colored melanoidins of larger molecular weights formed in the reaction of reducing sugars with peptides and proteins.

Theoretical Background

As this work is part of an ongoing project, the theoretical background is similar to that presented in previous research [2–9] and will be shown here for the sake of completeness. The chemical potential μ is defined within the conceptual framework of DFT [12,24] as:

$$\mu = \left(\frac{\partial E}{\partial N} \right)_{v(r)} = -\chi \quad (1)$$

where χ is the total electronegativity. In turn, the global hardness η is defined as:

$$\eta = \left(\frac{\partial^2 E}{\partial N^2} \right)_{v(r)} \quad (2)$$

If we consider the KID procedure mentioned in the introduction together with a finite difference approximation, then the above expressions can be written as:

$$\mu = -\frac{1}{2}(I + A) \approx \frac{1}{2}(\varepsilon_H + \varepsilon_L) \quad (3)$$

$$\eta = (I - A) \approx (\varepsilon_L - \varepsilon_H) \quad (4)$$

where ε_H and ε_L are the energies of HOMO and LUMO, respectively.

The electrophilicity index ω has been defined as [25]:

$$\omega = \frac{\mu^2}{2\eta} = \frac{(I + A)^2}{8(I - A)} \approx \frac{(\varepsilon_L + \varepsilon_H)^2}{8(\varepsilon_L - \varepsilon_H)} \quad (5)$$

Applying the same ideas, two definitions of Fukui functions depending on total electronic densities are obtained:

$$f^+(r) = \rho_{N+1}(r) - \rho_N(r) \quad (6)$$

$$f^-(r) = \rho_N(r) - \rho_{N-1}(r) \quad (7)$$

where $\rho_{N+1}(r)$, $\rho_N(r)$, and $\rho_{N-1}(r)$, are the electronic densities at point r for the system with $N+1$, N , and $N-1$ electrons, respectively. The first function, $f^+(r)$, has been associated to reactivity for a nucleophilic attack, and thus it measures the intramolecular reactivity at the site r towards a nucleophilic reagent. The second, $f^-(r)$, has been associated to reactivity for an electrophilic attack, and thus this function measures the intramolecular reactivity at the site r toward an electrophilic reagent [24].

Morell et al. [13,26–31] proposed a local reactivity descriptor (LRD), which is called the dual descriptor (DD): $f^{(2)}(r) \equiv \Delta f(r)$

$$\Delta f(r) = \left(\frac{\partial f(r)}{\partial N} \right)_{v(r)} \quad (8)$$

This can be condensed over the atomic sites: when $\Delta f_k > 0$, the process is driven by a nucleophilic attack on atom k , and then the atom acts as an electrophilic species; conversely, when $\Delta f_k < 0$, the process is driven by an electrophilic attack over atom k , and atom k acts as a nucleophilic species.

Finally, it should be noted that Domingo proposed the Parr functions $P(r)$ [32,33], whose definitions are given by the following equations:

$$P^-(r) = \rho_s^{rc} \quad (9)$$

for electrophilic attacks, and

$$P^+(r) = \rho_s^{ra} \quad (10)$$

for nucleophilic attacks, which are related to the atomic spin density (ASD) at the r atom of the radical cation or anion of a given molecule, respectively [34].

Settings and Computational Methods

Following the lines of our previous works [2–9], the computational studies were performed with the Gaussian 09 [35] series of programs with density functional methods as implemented in the computational package. The basis sets used in this work were Def2SVP for geometry optimization and frequencies, whereas Def2TZVP was considered for the calculation of the electronic properties [36,37]. All the calculations were performed in the presence of water as a solvent by performing integral equation formalism-polarized continuum model (IEF-PCM) computations according to the solvation model density (SMD) solvation model [38].

For the calculation of the molecular structures and properties of the studied systems, we chose ten density functionals that are known to consistently provide satisfactory results for several structural and thermodynamic properties:

CAM-B3LYP	Long-range-corrected B3LYP by the CAM method	[39]
LC- ω PBE	Long-range-corrected ω PBE density functional	[40]
M11	Range-separated hybrid meta-GGA	[41]
M11L	Dual-range local meta-GGA	[42]
MN12L	Non-separable local meta-NGA	[43]
MN12SX	Range-separated hybrid non-separable meta-NGA	[44]
N12	Non-separable local NGA	[45]
N12SX	Range-separated hybrid NGA	[44]
ω B97X	Long-range corrected density functional	[46]
ω B97XD	ω B97X version including empirical dispersion	[47]

In these functionals, GGA stands for generalized gradient approximation (in which the density functional depends on the up and down spin densities and their reduced gradient) and NGA stands for non-separable gradient approximation (in which the density functional depends on the up and down spin densities and their reduced gradient, and also adopts a non-separable form).

RESULTS AND DISCUSSIONS

This study took the molecular structures of the Red-M1 intermediate melanoidin pigment from PubChem (<https://pubchem.ncbi.nlm.nih.gov>), a public repository for information pertaining chemical substances together with the biological activities with which they are associated. The molecular structure with IUPAC Name is 1,4,6,9-tetracarboxymethyl-5-(1,2,3,4-tetrahydroxybutyl)-8-hydroxymethyl-3-(2,3-dihydroxy-propyl)-5,6-dihydro-pyrrolo[2',3':4,5]pyrrolo[2,3-e]pyrrolo[3,2-b]azepine-9-ium.Red-M2 was built as the diastereomer of the Red-M1 molecule. The pre-optimization of the resultant system involved selecting the most stable conformers. The selection was done using random sampling that involved molecular mechanics techniques and the inclusion of various torsional angles via the general MMFF94 force field [48–52] using the Marvin View 17.15 program, which is an advanced chemical viewer suited to multiple- and single-chemical queries, structures, and re-actions (<https://www.chemaxon.com>). Afterwards, the structures that the resultant lower-energy conformer assumed for each molecule were reoptimized using the ten density functionals mentioned in the previous section, together with the Def2SVP basis set as well as the SMD solvation model, in which the solvent was water.

The analysis of the results obtained in the study aimed at verifying that the KID procedure was fulfilled. On doing it previously, several descriptors associated with the results that the HOMO and LUMO calculations obtained are related with results obtained using the vertical I and A following the Δ SCF procedure. A link exists between the three main descriptors and the simplest conformity to the Koopmans' theorem by linking ϵ_H with -I, ϵ_L with -A, and their be-

havior in describing the HOMO–LUMO gap as $J_I = |\varepsilon H + E_{gs}(N-1) - E_{gs}(N)|$, $J_A = |\varepsilon L + E_{gs}(N) - E_{gs}(N+1)|$, and $J_{HL} = \sqrt{(J_I^2 + J_A^2)}$. Notably, the JA descriptor consists of an approximation that remains valid only when the HOMO that a radical anion has (the SOMO) shares similarity with the LUMO of the neutral system. Consequently, we decided to design another descriptor ΔSL , to guide in verifying the accuracy of the approximation.

Tables 1 and 2 illustrate the electronic energies of neutral, positive, and negative molecular systems of the Red-M1 and Red-M2 intermediate melanoidins; the HOMO, LUMO, and SOMO orbital energies (all in au); and the calculation of the J_I , J_A , J_{HL} , and ΔSL descriptors involves using the ten density functional as well as the Def2TZVP basis set with water as a solvent, which is simulated through the SMD parametrization of the IEF-PCM model.

Table 1. Electronic energies of the neutral, positive and negative molecular systems (in au) of Red-M1; the HOMO, LUMO and SOMO orbital energies (also in au); the J_I , J_A , J_{HL} and ΔSL descriptors calculated with the ten density functionals and the Def2TZVP basis set using water as a solvent, simulated with the SMD parametrization of the IEF-PCM model.

	E_0	E+	E-	HOMO	LUMO	SOMO	J_I	J_A	J_{HL}	ΔSL
CAM-B3LYP	-2432.5212	-2432.3343	-2432.6334	-0.2360	-0.0626	-0.1607	0.0490	0.0496	0.0697	0.0982
LC- ω PBE	-2432.0877	-2431.8951	-2432.2131	-0.2797	-0.0389	-0.2092	0.0871	0.0865	0.1227	0.1703
M11	-2432.3786	-2432.1828	-2432.4990	-0.2739	-0.0431	-0.1961	0.0781	0.0774	0.1100	0.1531
M11L	-2432.2581	-2432.0594	-2432.3776	-0.1905	-0.1296	-0.1101	0.0082	0.0101	0.0130	0.0196
MN12L	-2431.3635	-2431.1766	-2431.4687	-0.1792	-0.1136	-0.0979	0.0077	0.0085	0.0115	0.0157
MN12SX	-2431.5013	-2431.3063	-2431.6142	-0.1944	-0.1130	-0.1126	0.0006	0.0001	0.0006	0.0004
N12	-2433.1637	-2432.9889	-2433.2615	-0.1654	-0.1093	-0.0880	0.0095	0.0115	0.0149	0.0214
N12SX	-2432.4786	-2432.2928	-2432.5870	-0.1866	-0.1068	-0.1094	0.0008	0.0015	0.0017	0.0026
ω B97X	-2433.0096	-2432.8204	-2433.1264	-0.2692	-0.0370	-0.1949	0.0800	0.0798	0.1129	0.1579
ω B97XD	-2432.8597	-2432.6701	-2432.9735	-0.2583	-0.0444	-0.1822	0.0687	0.0694	0.0977	0.1378

Table 2. Electronic energies of the neutral, positive and negative molecular systems (in au) of Red-M2; the HOMO, LUMO and SOMO orbital energies (also in au); the J_I , J_A , J_{HL} and ΔSL descriptors calculated with the ten density functionals and the Def2TZVP basis set using water as a solvent, simulated with the SMD parametrization of the IEF-PCM model.

	E_0	E+	E-	HOMO	LUMO	SOMO	J_I	J_A	J_{HL}	ΔSL
CAM-B3LYP	-2432.5212	-2432.3343	-2432.6334	-0.2360	-0.0626	-0.1607	0.0490	0.0496	0.0697	0.0982
LC- ω PBE	-2432.0877	-2431.8951	-2432.2131	-0.2797	-0.0389	-0.2092	0.0871	0.0865	0.1227	0.1703
M11	-2432.3786	-2432.1828	-2432.4990	-0.2739	-0.0431	-0.1961	0.0781	0.0774	0.1100	0.1531
M11L	-2432.2581	-2432.0594	-2432.3776	-0.1905	-0.1296	-0.1101	0.0082	0.0101	0.0130	0.0196
MN12L	-2431.3636	-2431.1766	-2431.4687	-0.1792	-0.1136	-0.0979	0.0077	0.0085	0.0115	0.0157
MN12SX	-2431.5013	-2431.3063	-2431.6142	-0.1944	-0.1130	-0.1126	0.0006	0.0001	0.0006	0.0004
N12	-2433.1637	-2432.9889	-2433.2615	-0.1654	-0.1093	-0.0880	0.0095	0.0115	0.0149	0.0213
N12SX	-2432.4786	-2432.2928	-2432.5870	-0.1866	-0.1068	-0.1094	0.0008	0.0015	0.0017	0.0026
ω B97X	-2433.0096	-2432.8204	-2433.1264	-0.2692	-0.0370	-0.1949	0.0800	0.0798	0.1129	0.1579
ω B97XD	-2432.8597	-2432.6701	-2432.9735	-0.2583	-0.0444	-0.1822	0.0687	0.0694	0.0976	0.1378

Next, we consider four other descriptors that analyze how useful the studied density functionals are for the prediction of the electronegativity χ , global hardness η , and global electrophilicity ω . For a combination of these conceptual DFT descriptors, considering only the energies of the HOMO and LUMO or the vertical I and A: $J_\chi = |\chi - \chi_K|$, $J_\eta = |\eta - \eta_K|$, and $J_{CDFT} = \sqrt{((J_\chi^2 + J_\eta^2 + J_\omega^2))}$, where CDFT stands for conceptual DFT. The results of the calculations of J_χ , J_η , J_ω , and J_{CDFT} for the low-energy conformers of the Red-M1 and Red-M2 intermediate melanoidin pigments are displayed in Tables 3 and 4.

Table 3. $J\chi$, $J\eta$, $J\omega$, and J_{CDFT} for the Red-M1 intermediate melanoidin pigment.

	$J\chi$	$J\eta$	$J\omega$	J_{CDFT}
CAM-B3LYP	0.0003	0.0986	0.0852	0.1303
LC- ω PBE	0.0003	0.1736	0.1354	0.2201
M11	0.0004	0.1555	0.1115	0.1914
M11L	0.0010	0.0183	0.0505	0.0538
MN12L	0.0004	0.0162	0.0329	0.0367
MN12SX	0.0003	0.0007	0.0008	0.0011
N12	0.0010	0.0210	0.0477	0.0521
N12SX	0.0004	0.0024	0.0048	0.0054
ω B97X	0.0001	0.1597	0.1109	0.1945
ω B97XD	0.0004	0.1381	0.0983	0.1695

Table 4. $J\chi$, $J\eta$, $J\omega$, and J_{CDFT} for the Red-M2 intermediate melanoidin pigment.

	$J\chi$	$J\eta$	$J\omega$	J_{CDFT}
CAM-B3LYP	0.0003	0.0986	0.0852	0.1303
LC- ω PBE	0.0003	0.1736	0.1354	0.2201
M11	0.0004	0.1555	0.1115	0.1914
M11L	0.0010	0.0183	0.0505	0.0538
MN12L	0.0004	0.0162	0.0329	0.0367
MN12SX	0.0003	0.0007	0.0008	0.0011
N12	0.0010	0.0210	0.0477	0.0521
N12SX	0.0004	0.0023	0.0048	0.0054
ω B97X	0.0001	0.1597	0.1109	0.1945
ω B97XD	0.0004	0.1381	0.0983	0.1695

As Tables 1 to 4 show, the KID procedure applies accurately from the MN12SX and N12SX density functionals that are RS hybrid meta-NGA and RS hybrid NGA density functionals, respectively. In fact, the values of JI , JA , and JHL are not zero. Nevertheless, the results tend to be impressive, especially for the MN12SX density functional. Additionally, the ΔSL descriptor reaches the minimum values when the MN12SX and N12SX density functionals are used in the calculations. This implies that there is sufficient justification to assume that the LUMO of the neutral approximates the electron affinity.

The same density functionals follow the KID procedure in the rest of the descriptors, such as $J\chi$, $J\eta$, $J\omega$, and J_{CDFT} . The significance of these results is attributable to their illustration that reliance on JI , JA , and JHL would not be sufficient. For instance, if $J\chi$ were considered on its own to apply to each density functional covered in this study, the values would be considerably near zero. In the case of the other descriptors, only the MN12SX and N12SX density

functionals exhibit this behavior. This implies that the results from $J\chi$ are likely to be because of the cancellation of errors done by chance.

The Red-M1 and Red-M2 intermediate melanoidin pigments would be best studied using the time-dependent DFT (TDDFT), because the pigments are colored molecules. In the past, various TDDFT studies of molecules of different size have used optimally tuned RSH density functionals [23,53–71].

The considerable success of this approach is however undermined by the issue of tuning being system-dependent. Therefore, the focus should be on establishing the effectiveness of the behaviors of the fixed RSH density functionals in describing the excitation characteristics. Becke has recently mentioned that the adiabatic connection and the ideas of Hohenberg, Kohn, and Sham applying only to electronic ground states is a common misconception [72]. Furthermore, consistent with Baerends et al., the KS model is not appreciated for being superior because of its lowest

excitation energy in molecules. Physically, this amounts to an excitation of the KS system rather than electron addition, as would be the case in Hartree–Fock. Thus, it can be effectively used as a measure of the optical gap and is an effective approximation to the gap (in molecules) [73]. In their conclusion, van Meer et al. proposed that the HOMO–LUMO gap associated with the KS model tends to be an approximation of the lowest excitation energy, which is a desirable characteristic with no concerns regarding it [74].

Therefore, the calculation of the maximum wavelength absorption of the Red-M1 and Red-M2 pigments involved conducting ground-state calculations with the aforementioned ten density functionals at the same level of model chemistry and theory and determining the HOMO–LUMO gap. Figure 1 provides an illustration that graphically compares the results involved in the ground-state approximation derived from the HOMO–LUMO gap together with the experimental value of 564 nm for the Red-M1 molecule and 554 nm for the Red-M2 isomer [15].

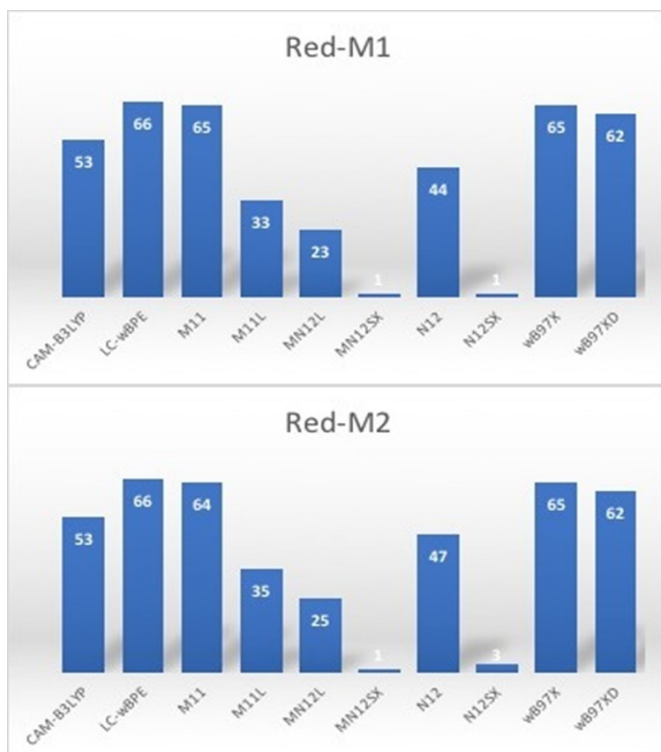


Figure 1. Graphical comparison of the results for the calculation of the λ_{\max} of the Red-M1 and Red-M2 pigments between the HOMO–LUMO gap and the

experimental data.

Notably, the presented results suggest that the differences with the experimental value for λ_{\max} tend to have the same order in the various functionals that the current study considers, apart from the N12 density functional. If the λ_{\max} values that the HOMO–LUMO gap generates were those considered, MN12SX and N12SX would appear to be especially accurate in predicting this value. This finding does not apply to the rest of the density functionals that this study considered.

These results can be explained by considering that both functionals have been built as the screened exchange (SX) version of range separation in which the electron exchange for small interelectronic distances is treated with a finite percentage of nonlocal HF exchange, but the nonlocality is screened at large distances, and electron exchange at long range is treated by a local approximation. This can be justified on the physical grounds that nonlocal exchange may be screened at long range by correlation effects and make those functionals as the perfect choice for predicting outer valence and Rydberg excitations. Moreover, it can be seen from Tables 1 to 4 that the values of the descriptors are very small in these cases and also the ΔSL values are also small meaning that the values of the energy of the LUMO are predicted accurately in addition to the HOMO energies.

Upon verifying that the MN12SX density functional has the tendency of peaking in calculating the global reactivity density descriptors and in predicting λ_{\max} , Figures 2 and 3 graphically present the optimized structures of the Red-M1 and Red-M2 pigments, as calculated based on the theory. Tables 5 and 7 illustrate the bond lengths, and Tables 6 and 8 demonstrate the bond angles.

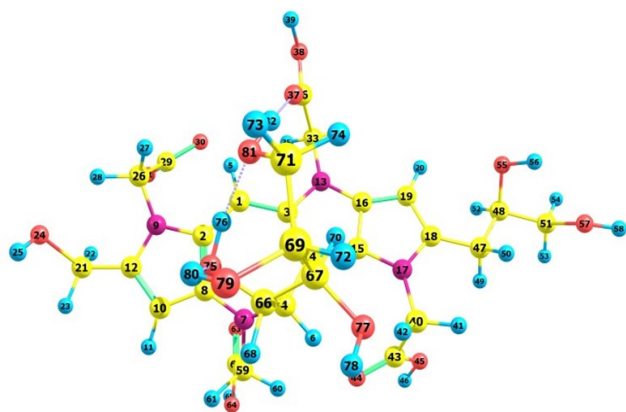


Figure 2. Schematic representation of the optimized structure of the Red-M1 pigment calculated with the MN12SX density functional showing the numbering of the atoms.

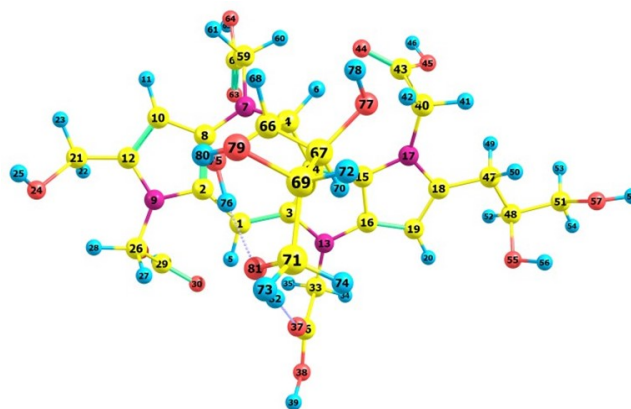


Figure 3. Schematic representation of the optimized structure of the Red-M2 pigment calculated with the MN12SX density functional showing the numbering of the atoms.

Table 5. Calculated bond lengths (in Å) of the Red-M1 intermediate melanoidin pigment with the MN12SX density functional.

Bond	Distance	Bond	Distance	Bond	Distance	Bond	Distance
R (1-2)	1.383	R (15-16)	1.417	R (36-38)	1.361	R (62-63)	1.219
R (1-3)	1.406	R (15-17)	1.386	R (38-39)	0.982	R (62-64)	1.372
R (1-5)	1.103	R (16-19)	1.414	R (40-41)	1.107	R (64-65)	0.982
R (2-8)	1.450	R (17-18)	1.384	R (40-42)	1.117	R (66-67)	1.540
R (2-9)	1.402	R (17-40)	1.447	R (40-43)	1.524	R (66-68)	1.124
R (3-13)	1.400	R (18-19)	1.397	R (43-44)	1.226	R (66-75)	1.442
R (3-14)	1.429	R (18-47)	1.497	R (43-45)	1.365	R (67-69)	1.545
R (4-6)	1.118	R (19-20)	1.093	R (45-46)	0.983	R (67-70)	1.122
R (4-7)	1.464	R (21-22)	1.114	R (47-48)	1.536	R (67-77)	1.457
R (4-14)	1.513	R (21-23)	1.114	R (47-49)	1.112	R (69-71)	1.536
R (4-66)	1.559	R (21-24)	1.438	R (47-50)	1.112	R (69-72)	1.120
R (7-8)	1.362	R (24-25)	0.981	R (48-51)	1.525	R (69-79)	1.442
R (7-59)	1.451	R (26-27)	1.111	R (48-52)	1.120	R (71-73)	1.115
R (8-10)	1.415	R (26-28)	1.109	R (48-55)	1.443	R (71-74)	1.114
R (9-12)	1.362	R (26-29)	1.527	R (51-53)	1.121	R (71-81)	1.447
R (9-26)	1.449	R (29-30)	1.225	R (51-54)	1.117	R (75-76)	1.003
R (10-11)	1.093	R (29-31)	1.363	R (51-57)	1.438	R (77-78)	0.983
R (10-12)	1.395	R (31-32)	0.983	R (55-56)	0.985	R (79-80)	0.988
R (12-21)	1.504	R (33-34)	1.108	R (57-58)	0.981	R (81-82)	0.987
R (13-16)	1.369	R (33-35)	1.113	R (59-60)	1.109	R (37-82)	1.940
R (13-33)	1.441	R (33-36)	1.522	R (59-61)	1.118	R (75-80)	1.965
R (14-15)	1.403	R (36-37)	1.227	R (59-62)	1.522	R (76-81)	1.700

Table 6. Calculated bond angles (in °) of the Red-M1 intermediate melanoidin pigment with the MN12SX density functional.

Bond	Angle	Bond	Angle	Bond	Angle	Bond	Angle
A (2-1-3)	123.6	A (9-26-28)	108.0	A (26-29-31)	114.4	A (63-62-64)	121.6
A (2-1-5)	118.0	A (9-26-29)	110.4	A (30-29-31)	121.6	A (62-64-65)	108.4
A (1-2-8)	130.7	A (11-10-12)	124.9	A (29-31-32)	108.8	A (67-66-68)	109.3
A (1-2-9)	122.3	A (10-12-21)	128.0	A (34-33-35)	107.3	A (67-66-75)	112.0
A (3-1-5)	118.1	A (12-21-22)	110.0	A (34-33-36)	109.7	A (66-67-79)	115.2
A (1-3-13)	122.3	A (12-21-23)	109.6	A (35-33-36)	109.2	A (66-67-70)	109.2
A (1-3-14)	128.7	A (12-21-24)	111.0	A (33-36-37)	124.8	A (66-67-77)	107.4
A (8-2-9)	105.8	A (16-13-33)	125.7	A (33-36-38)	113.8	A (68-66-75)	107.2
A (2-8-7)	127.4	A (13-16-15)	108.1	A (37-36-38)	121.4	A (66-75-76)	108.0
A (2-8-10)	106.9	A (13-16-19)	143.2	A (36-37-82)	163.0	A (66-75-80)	90.1
A (2-9-12)	110.3	A (13-33-34)	108.8	A (36-38-39)	109.0	A (69-67-70)	108.9
A (2-9-26)	124.1	A (13-33-35)	110.6	A (41-40-42)	108.8	A (69-67-77)	109.7
A (13-3-14)	108.9	A (13-33-36)	111.1	A (41-40-43)	110.0	A (67-69-71)	112.1

A (3-13-16)	108.5	A (14-15-16)	109.1	A (42-40-43)	109.9	A (67-69-72)	108.2
A (3-13-33)	125.8	A (14-15-17)	143.6	A (40-43-44)	124.6	A (67-69-79)	111.1
A (3-14-4)	127.2	A (16-15-17)	107.2	A (40-43-45)	114.3	A (70-67-77)	106.1
A (3-14-15)	105.4	A (15-16-19)	108.7	A (44-43-45)	121.1	A (67-77-78)	107.4
A (6-4-7)	106.8	A (15-17-18)	108.2	A (43-45-46)	108.7	A (71-69-72)	107.6
A (6-4-14)	106.9	A (15-17-40)	125.0	A (48-47-49)	109.4	A (71-69-79)	111.2
A (6-4-66)	107.6	A (16-19-18)	105.6	A (48-47-50)	108.9	A (69-71-73)	110.0
A (7-4-14)	111.3	A (16-19-20)	128.8	A (47-48-51)	111.0	A (69-71-74)	109.6
A (7-4-66)	110.2	A (18-17-40)	126.7	A (47-48-52)	109.5	A (69-71-81)	110.7
A (4-7-8)	122.8	A (17-18-19)	110.2	A (47-48-55)	109.9	A (72-69-79)	106.4
A (4-7-59)	117.6	A (17-18-47)	121.2	A (49-47-50)	106.2	A (69-79-80)	107.3
A (14-4-66)	113.6	A (17-40-41)	108.7	A (51-48-52)	110.1	A (73-71-74)	108.0
A (4-14-15)	127.2	A (17-40-42)	109.1	A (51-48-55)	108.4	A (73-71-81)	109.5
A (4-66-67)	110.7	A (17-40-43)	110.2	A (48-51-53)	110.9	A (74-71-81)	108.9
A (4-66-68)	107.5	A (19-18-47)	128.5	A (48-51-54)	110.4	A (71-81-82)	109.9
A (4-66-75)	110.1	A (18-19-20)	125.6	A (48-51-57)	107.3	A (71-81-76)	111.2
A (8-7-59)	118.2	A (18-47-48)	112.8	A (52-48-55)	107.8	A (76-75-80)	82.5
A (7-8-10)	125.6	A (18-47-49)	109.5	A (48-55-56)	105.9	A (75-76-81)	160.9
A (7-59-60)	109.2	A (18-47-50)	109.7	A (53-51-54)	107.6	A (79-80-75)	134.0
A (7-59-61)	111.4	A (22-21-23)	108.1	A (53-51-57)	110.4	A (81-82-37)	155.9
A (7-59-62)	110.5	A (22-21-24)	107.5	A (54-51-57)	110.0	A (82-81-76)	126.4
A (8-10-11)	127.1	A (23-21-24)	110.6	A (51-57-58)	108.1		
A (8-10-12)	107.9	A (21-24-25)	108.4	A (60-59-61)	107.1		
A (12-9-26)	125.7	A (27-26-28)	108.8	A (60-59-62)	108.9		
A (9-12-10)	109.0	A (27-26-29)	109.4	A (61-59-62)	109.6		
A (9-12-21)	123.0	A (28-26-29)	111.1	A (59-62-63)	125.0		
A (9-26-27)	109.1	A (26-29-30)	124.0	A (59-62-64)	113.4		

Table 7. Calculated bond lengths (in Å) of the Red-M2 intermediate melanoidin pigment with the MN12SX density functional.

Bond	Distance	Bond	Distance	Bond	Distance	Bond	Distance
R (1-2)	1.383	R (15-16)	1.417	R (36-38)	1.361	R (62-63)	1.219
R (1-3)	1.406	R (15-17)	1.386	R (38-39)	0.982	R (62-64)	1.372
R (1-5)	1.103	R (16-19)	1.414	R (40-41)	1.107	R (64-65)	0.982
R (2-8)	1.450	R (17-18)	1.384	R (40-42)	1.117	R (66-67)	1.540
R (2-9)	1.402	R (17-40)	1.447	R (40-43)	1.524	R (66-68)	1.124
R (3-13)	1.400	R (18-19)	1.397	R (43-44)	1.226	R (66-75)	1.442
R (3-14)	1.429	R (18-47)	1.497	R (43-45)	1.365	R (67-69)	1.545
R (4-6)	1.118	R (19-20)	1.093	R (45-46)	0.983	R (67-70)	1.122
R (4-7)	1.464	R (21-22)	1.114	R (47-48)	1.536	R (67-77)	1.457
R (4-14)	1.513	R (21-23)	1.114	R (47-49)	1.112	R (69-71)	1.536
R (4-66)	1.559	R (21-24)	1.438	R (47-50)	1.112	R (69-72)	1.120
R (7-8)	1.362	R (24-25)	0.981	R (48-51)	1.525	R (69-79)	1.442
R (7-59)	1.451	R (26-27)	1.111	R (48-52)	1.120	R (71-73)	1.115
R (8-10)	1.415	R (26-28)	1.109	R (48-55)	1.443	R (71-74)	1.114
R (9-12)	1.362	R (26-29)	1.527	R (51-53)	1.121	R (71-81)	1.447
R (9-26)	1.449	R (29-30)	1.225	R (51-54)	1.117	R (75-76)	1.003
R (10-11)	1.093	R (29-31)	1.363	R (51-57)	1.438	R (77-78)	0.983
R (10-12)	1.395	R (31-32)	0.983	R (55-56)	0.985	R (79-80)	0.988
R (12-21)	1.504	R (33-34)	1.108	R (57-58)	0.981	R (81-82)	0.987
R (13-16)	1.369	R (33-35)	1.113	R (59-60)	1.109	R (37-82)	1.940
R (13-33)	1.441	R (33-36)	1.522	R (59-61)	1.118	R (75-80)	1.965
R (14-15)	1.403	R (36-37)	1.227	R (59-62)	1.522	R (76-81)	1.700

Table 8. Calculated bond angles (in °) of the Red-M2 intermediate melanoidin pigment with the MN12SX density functional.

Bond	Angle	Bond	Angle	Bond	Angle	Bond	Angle
A (2-1-3)	123.6	A (9-26-28)	108.0	A (26-29-31)	114.4	A (63-62-64)	121.6
A (2-1-5)	118.0	A (9-26-29)	110.4	A (30-29-31)	121.6	A (62-64-65)	108.4
A (1-2-8)	130.7	A (11-10-12)	124.9	A (29-31-32)	108.8	A (67-66-68)	109.3
A (1-2-9)	122.3	A (10-12-21)	128.0	A (34-33-35)	107.3	A (67-66-75)	112.0
A (3-1-5)	118.1	A (12-21-22)	110.0	A (34-33-36)	109.7	A (66-67-79)	115.2
A (1-3-13)	122.3	A (12-21-23)	109.6	A (35-33-36)	109.2	A (66-67-70)	109.2
A (1-3-14)	128.7	A (12-21-24)	111.0	A (33-36-37)	124.8	A (66-67-77)	107.4
A (8-2-9)	105.8	A (16-13-33)	125.7	A (33-36-38)	113.8	A (68-66-75)	107.2
A (2-8-7)	127.4	A (13-16-15)	108.1	A (37-36-38)	121.4	A (66-75-76)	108.0
A (2-8-10)	106.9	A (13-16-19)	143.2	A (36-37-82)	163.0	A (66-75-80)	90.1

A (2-9-12)	110.3	A (13-33-34)	108.8	A (36-38-39)	109.0	A (69-67-70)	108.9
A (2-9-26)	124.1	A (13-33-35)	110.6	A (41-40-42)	108.8	A (69-67-77)	109.7
A (13-3-14)	108.9	A (13-33-36)	111.1	A (41-40-43)	110.0	A (67-69-71)	112.1
A (3-13-16)	108.5	A (14-15-16)	109.1	A (42-40-43)	109.9	A (67-69-72)	108.2
A (3-13-33)	125.8	A (14-15-17)	143.6	A (40-43-44)	124.6	A (67-69-79)	111.1
A (3-14-4)	127.2	A (16-15-17)	107.2	A (40-43-45)	114.3	A (70-67-77)	106.1
A (3-14-15)	105.4	A (15-16-19)	108.7	A (44-43-45)	121.1	A (67-77-78)	107.4
A (6-4-7)	106.8	A (15-17-18)	108.2	A (43-45-46)	108.7	A (71-69-72)	107.6
A (6-4-14)	106.9	A (15-17-40)	125.0	A (48-47-49)	109.4	A (71-69-79)	111.2
A (6-4-66)	107.6	A (16-19-18)	105.6	A (48-47-50)	108.9	A (69-71-73)	110.0
A (7-4-14)	111.3	A (16-19-20)	128.8	A (47-48-51)	111.0	A (69-71-74)	109.6
A (7-4-66)	110.2	A (18-17-40)	126.7	A (47-48-52)	109.5	A (69-71-81)	110.7
A (4-7-8)	122.8	A (17-18-19)	110.2	A (47-48-55)	109.9	A (72-69-79)	106.4
A (4-7-59)	117.6	A (17-18-47)	121.2	A (49-47-50)	106.2	A (69-79-80)	107.3
A (14-4-66)	113.6	A (17-40-41)	108.7	A (51-48-52)	110.1	A (73-71-74)	108.0
A (4-14-15)	127.2	A (17-40-42)	109.1	A (51-48-55)	108.4	A (73-71-81)	109.5
A (4-66-67)	110.7	A (17-40-43)	110.2	A (48-51-53)	110.9	A (74-71-81)	108.9
A (4-66-68)	107.5	A (19-18-47)	128.5	A (48-51-54)	110.4	A (71-81-82)	109.9
A (4-66-75)	110.1	A (18-19-20)	125.6	A (48-51-57)	107.3	A (71-81-76)	111.2
A (8-7-59)	118.2	A (18-47-48)	112.8	A (52-48-55)	107.8	A (76-75-80)	82.5
A (7-8-10)	125.6	A (18-47-49)	109.5	A (48-55-56)	105.9	A (75-76-81)	160.9
A (7-59-60)	109.2	A (18-47-50)	109.7	A (53-51-54)	107.6	A (79-80-75)	134.0
A (7-59-61)	111.4	A (22-21-23)	108.1	A (53-51-57)	110.4	A (81-82-37)	155.9
A (7-59-62)	110.5	A (22-21-24)	107.5	A (54-51-57)	110.0	A (82-81-76)	126.4
A (8-10-11)	127.1	A (23-21-24)	110.6	A (51-57-58)	108.1		
A (8-10-12)	107.9	A (21-24-25)	108.4	A (60-59-61)	107.1		
A (12-9-26)	125.7	A (27-26-28)	108.8	A (60-59-62)	108.9		
A (9-12-10)	109.0	A (27-26-29)	109.4	A (61-59-62)	109.6		
A (9-12-21)	123.0	A (28-26-29)	111.1	A (59-62-63)	125.0		
A (9-26-27)	109.1	A (26-29-30)	124.0	A (59-62-64)	113.4		

The electrodonating (ω^-) and electroaccepting (ω^+) powers have been defined as follows [75]:

$$\omega^- = \frac{(3I + A)^2}{16(I - A)} \approx \frac{(3\varepsilon H + \varepsilon L)^2}{16\eta_K} \quad (11)$$

And

$$\omega^+ = \frac{(I + 3A)^2}{16(I - A)} \approx \frac{(\varepsilon H + 3\varepsilon L)^2}{16\eta_K} \quad (12)$$

given that η_K is equal to the right side of Equation 4. Consequently, a higher ω^+ value is associated with improved inclination to accepting change. In contrast, a lower ω^- value represents improvement of the system as an electron donor. For comparisons of ω^+ and $-\omega^-$, the proposed definition of the net electrophilicity includes [76]:

$$\Delta\omega^\pm = \omega^+ - (-\omega^-) = \omega^+ + \omega^- \quad (13)$$

which represents the electroaccepting power in relation to the electrodonating power.

Table 9 illustrates the results obtained after calculat-

ing the electronegativity χ , chemical hardness η , global electrophilicity ω , electroaccepting ω^+ , and electrodonating ω^- powers, as well as the net electrophilicity with the MN12SX density functional. The Def2TZVP basis set is used with water acting as a solvent, in line with the SMD solvation model. It can be seen that the global descriptors cannot discriminate between the two isomers.

Table 9. Global reactivity descriptors for the Red-M1 and Red-M2 intermediate melanoidin pigments calculated with the MN12SX density functional.

	Electronegativity (χ)	Chemical Hardness (η)	Electrophilicity (ω)
Red-M1	4.1816	2.2154	3.9464
Red-M2	4.1816	2.2154	3.9464
	Electrodonating power (ω^-)	Electroaccepting power (ω^+)	Net electrophilicity ($\Delta\omega^\pm$)
Red-M1	5.9520	4.5597	10.5117
Red-M2	5.9520	4.5597	10.5117

The calculations of the condensed Fukui functions and DD have been done by using the Chemcraft molecular analysis program to extract the Mulliken and NPA atomic charges [77], beginning with single-point energy calculations involving the MN12SX density functional that uses the Def2TZVP basis set, also in line with the SMD solvation model, water is utilized as a solvent.

Considering the potential application of the Red-M1 and Red-M2 molecules as an antioxidant, it is of interest to get insight into the active sites for radical attack. A graphical representation of the radical Fukui function f^{ρ} is presented in Figures 4 and 5 for both isomers.

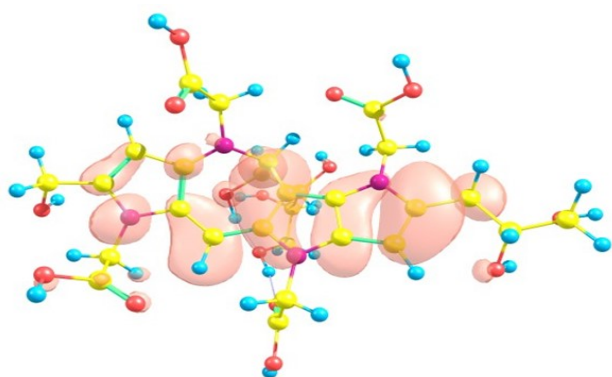


Figure 4. Graphical schematic representation of the radical Fukui function f^{ρ} of the Red-M1 intermediate melanoidin pigment.

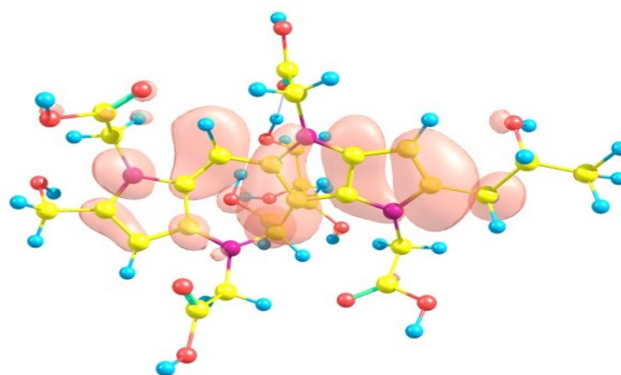


Figure 5. Graphical schematic representation of the radical Fukui function f^{ρ} of the Red-M2 intermediate melanoidin pigment.

The condensed electrophilic and nucleophilic Parr functions P_k^- and P_k^+ over the atoms of the Red-M1 and Red-M2 pigments have been calculated by extracting the Mulliken and Hirshfeld (or CM5) atomic charges using the Chemcraft molecular analysis program [77], starting from single-point energy calculations of the ionic species with the MN12SX density functional using the Def2TZVP basis set in the presence of water as a solvent, according to the SMD solvation model.

The results for the condensed DD calculated with Mulliken and NPA atomic charges, $\Delta f_k(M)$ and $\Delta f_k(N)$, as well as the electrophilic and nucleophilic Parr functions with Mulliken atomic charges, $P_k^-(M)$, $P_k^+(M)$, and with Hirshfeld (or CM5) atomic charges $P_k^-(H)$ and $P_k^+(H)$, are displayed in Tables 10 and 11 for Red-M1 and Red-M2, respectively.

Table 10. Condensed dual descriptor calculated with Mulliken atomic charges $\Delta f_k(M)$ and with NPA atomic charges $\Delta f_k(N)$, the electrophilic and nucleophilic Parr functions with Mulliken atomic charges, $P_k^-(M)$, $P_k^+(M)$, and with Hirshfeld (or CM5) atomic charges, $P_k^-(H)$ and $P_k^+(H)$ for the Red-M1 molecule. Only the values of Δf_k for which the absolute values is greater than 5 are displayed because lower values are not of significance for the chemical reactivity.

Atom	$\Delta f_k(M)$	$\Delta f_k(N)$	$P_k^+(M)$	$P_k^-(M)$	$P_k^+(H)$	$P_k^-(H)$
1C	22.24	17.19	0.4098	-0.1634	0.2159	-0.0401
2C	-10.74	-10.22	-0.0904	0.2599	0.0184	0.1499
3C	-13.51	-9.69	-0.1356	0.2527	-0.0046	0.1421
8C	7.07	6.76	0.2303	0.0257	0.1276	0.0560
12C	7.44	5.34	0.2223	0.0625	0.1345	0.0440
14C	6.38	5.66	0.2390	-0.0006	0.1120	0.0331
15C	-5.26	-4.85	-0.0482	0.1110	0.0090	0.0790
19C	-5.75	-4.43	-0.0495	0.0361	-0.0039	0.0528

Table 11. Condensed dual descriptor calculated with Mulliken atomic charges $\Delta f_k(M)$ and with NPA atomic charges $\Delta f_k(N)$, the electrophilic and nucleophilic Parr functions with Mulliken atomic charges, $P_k^-(M)$ and $P_k^+(M)$ and with Hirshfeld (or CM5) atomic charges, $P_k^-(H)$ and $P_k^+(H)$, for the Red-M2 molecule. Only the values of Δf_k for which the absolute values is greater than 1 are displayed because lower values are not of significance for the chemical reactivity.

Atom	$\Delta f_k(M)$	$\Delta f_k(N)$	$P_k^+(M)$	$P_k^-(M)$	$P_k^+(H)$	$P_k^-(H)$
1C	22.24	17.19	0.4098	-0.1634	0.2159	-0.0401
2C	-10.74	-10.23	-0.0904	0.2599	0.0184	0.1499
3C	-13.51	-9.69	-0.1356	0.2527	-0.0046	0.1421
8C	7.07	6.76	0.2303	0.0257	0.1276	0.0560
12C	7.44	5.34	0.2223	0.0625	0.1345	0.0440
14C	6.38	5.66	0.2390	-0.0006	0.1120	0.0330
15C	-5.26	-4.85	-0.0482	0.1110	0.0090	0.0790
19C	-5.75	-4.43	-0.0495	0.0361	-0.0039	0.0528

From the results for the local descriptors in Table 10 and 11, it can be concluded that C1 will be the preferred site for a nucleophilic attack and that this atom will act as an electrophilic species in a chemical reaction. In turn, it can be determined that C2 and C3 will be prone to electrophilic attacks and that these atomic sites will act as nucleophilic species in chemical reactions in which the Red-M1 and Red-M2 molecules are involved.

All calculations have been performed in the gas phase also in order to check the effect of the solvent in the prediction of the λ_{\max} and the local chemical reactivity of the melanoidins. The main conclusion is that there are not great differences between the results in either case. However, we believe that it is preferably to keep the results in the solvent phase because they are a better representation of the real chemical phenomena.

Unfortunately, the only experimental results available are those for the λ_{\max} of the melanoidins Red-M1 and Red-M2. Our predictions for the chemical reactivity should be validated in the future but we believe that the comparisons between the CDFT descriptors (the Fukui functions and the Dual Descriptor) and the MEDT descriptors (the Parr functions) and the good agreement between them is a good reason to make us confidence that our results are very accurate.

CONCLUSIONS

The ten fixed RSH density functionals, including CAM-B3LYP, LC- ω PBE, M11, M11L, MN12L, MN12SX, N12, N12SX, ω B97X, and ω B97XD were examined to establish whether they fulfill the empirical KID procedure. The assessment was performed by comparing the values from HOMO and LUMO calculations to those that the Δ SCF technique generates for the Red-M1 and Red-M2 molecules. These are intermediate melanoidin pigments that are of both academic and industrial interest. The study observed that the RS and hybrid meta-NGA MN12SX and N12SX density functionals tend to be the most suited in meeting this goal. In this case, they emerge as suitable alternatives to the density functionals once it is established that the behaviors of the functionals are tuned using a gap-fitting procedure. They also exhibit desirable prospects of how they will benefit future studies in understanding the chemical reactivity of colored melanoidins with larger molecular weights when reducing sugars react with proteins and peptides.

From the results of this work, it becomes evident that it is easy to predict the sites of interaction of the Red-M1 and Red-M2 pigments under study. This would involve having DFT-based reactivity descriptors including Parr functions and DD calculations. Evidently, the descriptors were useful in characterizing and describing the preferred reactive sites. They were also useful in comprehensively explaining the reactivity of the molecules.

Furthermore, it is also possible to predict the maximum absorption wavelength for the Red-M1 and Red-M2 pigments with considerable accuracy. The prediction would involve the MN12SX density functional beginning with the HOMO–LUMO gap instead of TDDFT calculations. This finding is particularly crucial considering its likelihood of being used to inform an alternative determination method for the color of larger systems such as prosthetic chromophore groups. This would become necessary in circumstances in which the TDDFT calculations would be prohibitive.

AUTHOR'S CONTRIBUTIONS

Daniel Glossman-Mitnik conceived and designed the research and headed, wrote, and revised the manuscript; J. Frau contributed to the writing and the revision of the article.

ACKNOWLEDGEMENTS

This work has been partially supported by CIMAV, SC and Consejo Nacional de Ciencia y Tecnología (CONACYT, Mexico) through Grant 219566-2014 for Basic Science Research. Daniel Glossman-Mitnik conducted this work while a Visiting Lecturer at the University of the Balearic Islands from which support is gratefully acknowledged. This work was co-funded by the Ministerio de Economía y Competitividad (MINECO) and the European Fund for Regional Development (FEDER) (CTQ2014-55835-R).

REFERENCES

1. Peverati, R., Truhlar, D.G.: Exchange-Correlation Functional with Good Accuracy for Both Structural and Energetic Properties while Depending Only on the Density and Its Gradient. *Journal of Chemical Theory and Computation* 8(7), 2310–2319 (2012) PMID:26588964 [View Article](#) [PubMed/NCBI](#)
2. Peverati, R., Truhlar, D.G.: Screened-Exchange Density Functionals with Broad Accuracy for Chemistry and Solid-State Physics. *Physical Chemistry Chemical Physics* 14(47), 16187–16191 (2012) PMID:23132141 [View Article](#) [PubMed/NCBI](#)
3. Peverati, R., Truhlar, D.G.: An Improved and Broadly Accurate Local Approximation to the Exchange-Correlation Density Functional: the MN12-L Functional for Electronic Structure Calculations in Chemistry and Physics. *Physical Chemistry Chemical Physics* 14(38), 13171–13174 (2012) PMID:22910998 [View Article](#) [PubMed/NCBI](#)
4. Peverati, R., Truhlar, D.G.: M11-L: A Local Density Functional That Provides Improved Accuracy for Electronic Structure Calculations in Chemistry and Physics. *The Journal of Physical Chemistry Letters* 3(1), 117–124 (2012) [View Article](#)
5. Peverati, R., Truhlar, D.G.: Improving the Accuracy of Hybrid Meta-GGA Density Functionals by Range Separation. *The Journal of Physical Chemistry Letters* 2(21), 2810–2817 (2011) [View Article](#)
6. Henderson, T.M., Izmaylov, A.F., Scalmani, G., Scuseria, G.E.: Can Short-Range Hybrids Describe Long-Range-Dependent Properties? *The Journal of Chemical Physics* 131(4), 044108 (2009) PMID:19655838 [View Article](#) [PubMed/NCBI](#)
7. Yanai, T., Tew, D.P., Handy, N.C.: A New Hybrid Exchange-Correlation Functional Using the Coulomb-Attenuating Method (CAM-B3LYP). *Chemical Physics Letters* 393(1-3), 51–57 (2004) [View Article](#)
8. Marenich, A., Cramer, C., Truhlar, D.: Universal Solvation Model Based on Solute Electron Density and a Continuum Model of the Solvent Defined by the Bulk Dielectric Constant and Atomic Surface Tensions. *Journal of Physical Chemistry B* 113, 6378–6396 (2009) PMID:19366259 [View Article](#) [PubMed/NCBI](#)
9. Weigend, F.: Accurate Coulomb-fitting Basis Sets for H to R. *Physical Chemistry Chemical Physics* 8, 1057–1065 (2006) PMID:16633586 [View Article](#) [PubMed/NCBI](#)
10. Weigend, F., Ahlrichs, R.: Balanced Basis Sets of Split Valence, Triple Zeta Valence and Quadruple Zeta Valence Quality for H to Rn: Design and Assessment of Accuracy. *Physical Chemistry Chemical Physics* 7, 3297–3305 (2005) Mid:16240044 [View Article](#) [PubMed/NCBI](#)
11. Frisch, M.J., Trucks, G.W., Schlegel, H.B., Scuseria, G.E., Robb, M.A., Cheeseman, J.R., Scalmani, G., Barone, V., Mennucci, B., Petersson, G.A., Nakatsuji, H., Caricato, M., Li, X., Hratchian, H.P., Izmaylov, A.F., Bloino, J., Zheng, G., Sonnenberg, J.L., Hada, M., Ehara, M., Toyota, K., Fukuda, R., Hasegawa, J., Ishida, M., Nakajima, T., Honda, Y., Kitao, O., Nakai, H., Vreven, T., Montgomery, J.A. Jr., Peralta, J.E., Ogliaro, F., Bearpark, M., Heyd, J.J., Brothers, E., Kudin, K.N., Staroverov, V.N., Kobayashi, R., Normand, J.,

- Raghavachari, K., Rendell, A., Burant, J.C., Iyengar, S.S., Tomasi, J., Cossi, M., Rega, N., Millam, J.M., Klene, M., Knox, J.E., Cross, J.B., Bakken, V., Adamo, C., Jaramillo, J., Gomperts, R., Stratmann: Gaussian 09 Revision E.01. Gaussian Inc., Wallingford CT, 2016
12. Domingo, L.R., Ríos-Gutiérrez, M., Pérez, P.: Applications of the Conceptual Density Functional Theory Indices to Organic Chemistry Reactivity. *Molecules* 21, 748 (2016) PMID:27294896 PMCID:PMC6273244 [View Article](#) [PubMed/NCBI](#)
 13. Chamorro, E., Pérez, P., Domingo, L.R.: On the Nature of Parr Functions to Predict the Most Reactive Sites along Organic Polar Reactions. *Chemical Physics Letters* 582, 141–143 (2013) [View Article](#)
 14. Domingo, L.R., Pérez, P., Sáez, J.A.: Understanding the Local Reactivity in Polar Organic Reactions through Electrophilic and Nucleophilic Parr Functions. *RSC Advances* 3, 1486–1494 (2013) [View Article](#)
 15. Morell, C., Hocquet, A., Grand, A., Jamart-Grégoire, B.: A Conceptual DFT Study of Hydrazino Peptides: Assessment of the Nucleophilicity of the Nitrogen Atoms by Means of the Dual Descriptor $\Delta f(r)$. *Journal of Molecular Structure: THEOCHEM* 849, 46–51 (2008) [View Article](#)
 16. Morell, C., Ayers, P.W., Grand, A., Gutiérrez-Oliva, S., Toro-Labbé, A.: Rationalization of the Diels-Alder Reactions through the Use of the Dual Reactivity Descriptor $\Delta f(r)$. *Physical Chemistry Chemical Physics* 10, 7239–7246 (2008) PMID:19060968 [View Article](#) [PubMed/NCBI](#)
 17. Ayers, P.W., Morell, C., De Proft, F., Geerlings, P.: Understanding the Woodward-Hoffmann Rules by Using Changes in Electron Density. *Chemistry - A European Journal* 13, 8240–8247 (2007) PMID:17639522 [View Article](#) [PubMed/NCBI](#)
 18. Cárdenas, C., Rabi, N., Ayers, P.W., Morell, C., Jaramillo, P., Fuentealba, P.: Chemical Reactivity Descriptors for Ambiphilic Reagents: Dual Descriptor, Local Hypersoftness, and Electrostatic Potential. *Journal of Physical Chemistry A* 113, 8660–8667 (2009) PMID:19580251 [View Article](#) [PubMed/NCBI](#)
 19. Morell, C., Grand, A., Toro-Labbé, A.: Theoretical Support for Using the $\Delta f(r)$ Descriptor. *Chemical Physics Letters* 425, 342–346 (2006) [View Article](#)
 20. Morell, C., Grand, A., Toro-Labbé, A.: New Dual Descriptor for Chemical Reactivity. *Journal of Physical Chemistry A* 109, 205–212 (2005) PMID:16839107 [View Article](#) [PubMed/NCBI](#)
 21. Parr, R.G., Szentpaly, L.V., Liu, S.B.: Electrophilicity Index. *Journal of the American Chemical Society* 121, 1922–1924 (1999) [View Article](#)
 22. Parr, R.G., Yang, W.: Density Functional Approach to the Frontier-Electron Theory of Chemical Reactivity. *Journal of the American Chemical Society* 106, 4049–4050 (1984) [View Article](#)
 23. Jacquemin, D., Moore, B., Planchat, A., Adamo, C., Autschbach, J.: Performance of an Optimally Tuned Range-Separated Hybrid Functional for 0-0 Electronic Excitation Energies. *Journal of Chemical Theory and Computation* 10(4), 1677–1685 (2014) PMID:26580376 [View Article](#) [PubMed/NCBI](#)
 24. Cramer, C.J.: *Essentials of Computational Chemistry - Theories and Models*, 2nd edn. John Wiley & Sons, Chichester, England (2004)
 25. Gledhill, J.D., De Proft, F., Tozer, D.J.: Range-Separation Parameter in Tuned Exchange-Correlation Functionals: Successive Ionizations and the Fukui Function. *Journal of Chemical Theory and Computation* 12(10), 4879–4884 (2016) PMID:27622316 [View Article](#) [PubMed/NCBI](#)
 26. Jensen, F.: *Introduction to Computational Chemistry*, 2nd edn. John Wiley & Sons, Chichester, England (2007)
 27. Lewars, E.: *Computational Chemistry - Introduction to the Theory and Applications of Molecular and Quantum Mechanics*. Kluwer Academic Publishers, Dordrecht (2003)
 28. Young, D.C.: *Computational Chemistry - A Practical Guide for Applying Techniques to Real-World Problems*. John Wiley & Sons, New York (2001)
 29. Easton, R.E., Giesen, D.J., Welch, A., Cramer, C.J., Truhlar, D.G.: The MIDI! Basis Set for Quantum Mechanical Calculations of Molecular Geometries and Partial Charges. *Theoretical Chemistry Accounts* 93, 281–301 (1996) [View Article](#)
 30. Huzinaga, S., Andzelm, J., Klobukowski, M., Radzio-Audzelm, E., Sakai, Y., Tatewaki, H.: *Gaussian Basis Sets for Molecular Calculations*. Elsevier, Amsterdam (1984)
 31. Shirahashi, Y., Watanabe, H., Hayase, F.: Identification of Red Pigments Formed in a D-Xylose-Glycine Reaction System. *Bioscience, Biotechnology and Biochemistry* 73(10), 2287–2292 (2009) PMID:19809196 [View Article](#) [PubMed/NCBI](#)
 32. Toro-Labbé, A. (ed.): *Theoretical Aspects of*

- Chemical Reactivity. Elsevier Science, Amsterdam (2007)
33. Chattaraj, P.K. (ed.): *Chemical Reactivity Theory - A Density Functional View*. CRC Press. Taylor & Francis Group, Boca Raton (2009)
 34. Parr, R.G., Yang, W.: *Density-Functional Theory of Atoms and Molecules*. Oxford University Press, New York (1989)
 35. Geerlings, P., De Proft, F., Langenaeker, W.: *Conceptual Density Functional Theory*. *Chemical Reviews* 103, 1793–1873 (2003) PMID:12744694 [View Article](#) [PubMed/NCBI](#)
 36. Nursten, H. (ed.): *The Maillard Reaction - Chemistry, Biochemistry and Implications*. The Royal Society of Chemistry, Cambridge, UK (2005)
 37. Frau, J., Flores-Holguín, N., Glossman-Mitnik, D.: Chemical Reactivity Properties, pKa Values, AGEs Inhibitor Abilities and Bioactivity Scores of the Mirabamides A–H Peptides of Marine Origin Studied by Means of Conceptual DFT. *Marine Drugs* 16(9), 302–19 (2018) PMID:30154377 PMCid:PMC6163382 [View Article](#) [PubMed/NCBI](#)
 38. Frau, J., Glossman-Mitnik, D.: Blue M2: An Intermediate Melanoidin Studied via Conceptual DFT. *Journal of Molecular Modeling* 24 (138), 1–13 (2018) [View Article](#)
 39. Frau, J., Glossman-Mitnik, D.: Chemical Reactivity Theory Applied to the Calculation of the Local Reactivity Descriptors of a Colored Maillard Reaction Product. *Chemical Science International Journal* 22(4), 1–14 (2018) [View Article](#)
 40. Frau, J., Glossman-Mitnik, D.: Computational Study of the Chemical Reactivity of the Blue-M1 Intermediate Melanoidin. *Computational and Theoretical Chemistry* 1134, 22–29 (2018) [View Article](#)
 41. Frau, J., Glossman-Mitnik, D.: Molecular Reactivity of some Maillard Reaction Products Studied through Conceptual DFT. *Contemporary Chemistry* 1(1), 1–14 (2018)
 42. Frau, J., Glossman-Mitnik, D.: Conceptual DFT Study of the Local Chemical Reactivity of the Colored BISARG Melanoidin and Its Protonated Derivative. *Frontiers in Chemistry* 6(136), 1–9 (2018) [View Article](#)
 43. Frau, J., Glossman-Mitnik, D.: Molecular Reactivity and Absorption Properties of Melanoidin Blue-G1 through Conceptual DFT. *Molecules* 23(3), 559–15 (2018) PMID:29498665 PMCid:PMC6017537 [View Article](#) [PubMed/NCBI](#)
 44. Frau, J., Glossman-Mitnik, D.: Conceptual DFT Study of the Local Chemical Reactivity of the Dilysyldipyrrolones A and B Intermediate Melanoidins. *Theoretical Chemistry Accounts* (5), 1210 (2018) [View Article](#)
 45. Argirova, M.D.: Photosensitizer Activity of Model Melanoidins. *Journal of Agricultural and Food Chemistry* 53(4), 1210–1214 (2005) PMID:15713043 [View Article](#) [PubMed/NCBI](#)
 46. Chai, J., Head-Gordon, M.: Systematic Optimization of Long-Range Corrected Hybrid Density Functionals. *Journal of Chemical Physics* 128, 084106 (2008) PMID:18315032 [View Article](#) [PubMed/NCBI](#)
 47. Chai, J., Head-Gordon, M.: Long-Range Corrected Hybrid Density Functionals with Damped Atom-Atom Dispersion Corrections. *Physical Chemistry Chemical Physics* 10, 6615–6620 (2008) PMID:18989472 [View Article](#) [PubMed/NCBI](#)
 48. Halgren, T.A.: Merck Molecular Force Field. I. Basis, Form, Scope, Parameterization, and Performance of MMFF94. *Journal of Computational Chemistry* 17(5-6), 490–519 (1996) 1096-987X(199604)17:5/6<490::AID-JCC1>3.0.CO;2-P [View Article](#)
 49. Halgren, T.A.: Merck Molecular Force Field. II. MMFF94 van der Waals and Electrostatic Parameters for Intermolecular Interactions. *Journal of Computational Chemistry* 17(5-6), 520–552 (1996) 1096-987X(199604)17:5/6<520::AID-JCC2>3.0.CO;2-W [View Article](#)
 50. Halgren, T.A.: MMFF VI. MMFF94s Option for Energy Minimization Studies. *Journal of Computational Chemistry* 20(7), 720–729 (1999) 1096-987X(199905)20:7<720::AID-JCC7>3.0.CO;2-X [View Article](#)
 51. Halgren, T.A., Nachbar, R.B.: Merck Molecular Force Field. IV. Conformational Energies and Geometries for MMFF94. *Journal of Computational Chemistry* 17(5-6), 587–615 (1996) 1096-987X(199604)17:5/6<587::AID-JCC4>3.0.CO;2-Q [View Article](#)
 52. Halgren, T.A.: Merck Molecular Force field. V. Extension of MMFF94 Using Experimental Data, Additional Computational Data, and Empirical Rules. *Journal of Computational Chemistry* 17(5-6), 616–641 (1996) 1096-987X(199604)17:5/6<616::AID-JCC5>3.0.CO;2-X [View Article](#)
 53. Egger, D.A., Weissman, S., Refaely-Abramson, S., Sharifzadeh, S., Dauth, M., Baer, R., Kummel, S., Neaton, J.B., Zojer, E., Kronik, L.: Outer-Valence Electron Spectra of Prototypical Aromatic Heterocycles From an Optimally Tuned Range-Separated Hybrid Functional. *Journal of Chemical Theory and Compu-*

- tation 10(5), 1934–1952 (2014)
PMid:24839410 PMCid:PMC4020925 [View Article](#) [PubMed/NCBI](#)
54. Foster, M.E., Wong, B.M.: Nonempirically Tuned Range-Separated DFT Accurately Predicts Both Fundamental and Excitation Gaps in DNA and RNA Nucleobases. *Journal of Chemical Theory and Computation* 8(8), 2682–2687 (2012) PMid:22904693 PMCid:PMC3419459 [View Article](#) [PubMed/NCBI](#)
55. Foster, M.E., Azoulay, J.D., Wong, B.M., Alendorff, M.D.: Novel Metal–Organic Framework Linkers for Light Harvesting Applications. *Chemical Science* 5(5), 2081–2090 (2014) [View Article](#)
56. Karolewski, A., Stein, T., Baer, R., Kummel, S.: Communication: Tailoring the Optical Gap in Light-Harvesting Molecules. *The Journal of Chemical Physics* 134(15), 151101–5 (2011) PMid:21513368 [View Article](#) [PubMed/NCBI](#)
57. Karolewski, A., Kronik, L., Kummel, S.: Using Optimally Tuned Range Separated Hybrid Functionals in Ground-State Calculations: Consequences and Caveats. *The Journal of Chemical Physics* 138(20), 204115 (2013) PMid:23742462 [View Article](#) [PubMed/NCBI](#)
58. Koppen, J.V., Hapka, M., Szczeniak, M.M., Chalasiński, G.: Optical Absorption Spectra of Gold Clusters Au(n) (n = 4, 6, 8, 12, 20) From Long-Range Corrected Functionals with Optimal Tuning. *The Journal of Chemical Physics* 137(11), 114302 (2012) PMid:22998257 [View Article](#) [PubMed/NCBI](#)
59. Kronik, L., Stein, T., Refaely-Abramson, S., Baer, R.: Excitation Gaps of Finite-Sized Systems from Optimally Tuned Range-Separated Hybrid Functionals. *Journal of Chemical Theory and Computation* 8(5), 1515–1531 (2012) PMid:26593646 [View Article](#) [PubMed/NCBI](#)
60. Kuritz, N., Stein, T., Baer, R., Kronik, L.: Charge-Transfer-Like $\pi \rightarrow \pi^*$ Excitations in Time-Dependent Density Functional Theory: A Conundrum and Its Solution. *Journal of Chemical Theory and Computation* 7(8), 2408–2415 (2011) PMid:26606616 [View Article](#) [PubMed/NCBI](#)
61. Lima, I.T., Prado, A.d.S., Martins, J.B.L., de Oliveira Neto, P.H., Ceschin, A.M., da Cunha, W.F., da Silva Filho, D.A.: Improving the Description of the Optical Properties of Carotenoids by Tuning the Long-Range Corrected Functionals. *The Journal of Physical Chemistry A* 120(27), 4944–4950 (2016) PMid:26885879 [View Article](#) [PubMed/NCBI](#)
62. Manna, A.K., Lee, M.H., McMahon, K.L., Dunietz, B.D.: Calculating High Energy Charge Transfer States Using Optimally Tuned Range-Separated Hybrid Functionals. *Journal of Chemical Theory and Computation* 11(3), 1110–1117 (2015) PMid:26579761 [View Article](#) [PubMed/NCBI](#)
63. Moore II, B., Autschbach, J.: Longest-Wavelength Electronic Excitations of Linear Cyanines: The Role of Electron Delocalization and of Approximations in Time-Dependent Density Functional Theory. *Journal of Chemical Theory and Computation* 9(11), 4991–5003 (2013) PMid:26583416 [View Article](#) [PubMed/NCBI](#)
64. Niskanen, M., Hukka, T.I.: Modeling of Photoactive Conjugated Donor-Acceptor Copolymers: the Effect of the Exact HF Exchange in DFT Functionals on Geometries and Gap Energies of Oligomer and Periodic Models. *Phys. Chem. Chem. Phys.* 16(26), 13294–13305 (2014) [View Article](#)
65. Pereira, T.L., Leal, L.A., da Cunha, W.F., Timóteo de Sousa Júnior, R., Ribeiro Junior, L.A., Antonio da Silva Filho, D.: Optimally Tuned Functionals Improving the Description of Optical and Electronic Properties of the Phthalocyanine Molecule. *Journal of Molecular Modeling* 23(3), 71 (2017) PMid:28197842 [View Article](#) [PubMed/NCBI](#)
66. Phillips, H., Zheng, S., Hyla, A., Laine, R., Goodson III, T., Geva, E., Dunietz, B.D.: Ab Initio Calculation of the Electronic Absorption of Functionalized Octahedral Silsesquioxanes via Time-Dependent Density Functional Theory with Range-Separated Hybrid Functionals. *The Journal of Physical Chemistry A* 116(4), 1137–1145 (2012) PMid:22191709 [View Article](#) [PubMed/NCBI](#)
67. Phillips, H., Geva, E., Dunietz, B.D.: Calculating Off-Site Excitations in Symmetric Donor-Acceptor Systems via Time-Dependent Density Functional Theory with Range-Separated Density Functionals. *Journal of Chemical Theory and Computation* 8(8), 2661–2668 (2012) PMid:26592111 [View Article](#) [PubMed/NCBI](#)
68. Refaely-Abramson, S., Baer, R., Kronik, L.: Fundamental and Excitation Gaps in Molecules of Relevance for Organic Photovoltaics From an Optimally Tuned Range-Separated Hybrid Functional. *Physical Review B* 84(7), 075144–8 (2011) [View Article](#)
69. Stein, T., Kronik, L., Baer, R.: Prediction of Charge-Transfer Excitations in Coumarin-Based Dyes Using a Range-Separated Functional Tuned From First Principles. *The Journal*

- of Chemical Physics 131(24), 244119 (2009) PMID:20059066 [View Article](#) [PubMed/NCBI](#)
70. Stein, T., Kronik, L., Baer, R.: Reliable Prediction of Charge Transfer Excitations in Molecular Complexes Using Time-Dependent Density Functional Theory. *Journal of the American Chemical Society* 131(8), 2818–2820 (2009) PMID:19239266 [View Article](#) [PubMed/NCBI](#)
71. Sun, H., Autschbach, J.: Electronic Energy Gaps for π -Conjugated Oligomers and Polymers Calculated with Density Functional Theory. *Journal of Chemical Theory and Computation* 10(3), 1035–1047 (2014) PMID:26580181 [View Article](#) [PubMed/NCBI](#)
72. Becke, A.D.: Vertical Excitation Energies From the Adiabatic Connection. *The Journal of Chemical Physics* 145(19), 194107 (2016) PMID:27875864 [View Article](#) [PubMed/NCBI](#)
73. Baerends, E.J., Gritsenko, O.V., van Meer, R.: The Kohn-Sham Gap, the Fundamental Gap and the Optical Gap: The Physical Meaning of Occupied and Virtual Kohn-Sham Orbital Energies. *Physical Chemistry Chemical Physics* 15(39), 16408–16425 (2013) PMID:24002107 [View Article](#) [PubMed/NCBI](#)
74. van Meer, R., Gritsenko, O.V., Baerends, E.J.: Physical Meaning of Virtual Kohn-Sham Orbitals and Orbital Energies: An Ideal Basis for the Description of Molecular Excitations. *Journal of Chemical Theory and Computation* 10(10), 4432–4441 (2014) PMID:26588140 [View Article](#) [PubMed/NCBI](#)
75. Gázquez, J.L., Cedillo, A., Vela, A.: Electron-donating and Electroaccepting Powers. *Journal of Physical Chemistry A* 111(10), 1966–1970 (2007) PMID:17305319 [View Article](#) [PubMed/NCBI](#)
76. Chattaraj, P.K., Chakraborty, A., Giri, S.: Net Electrophilicity. *Journal of Physical Chemistry A* 113(37), 10068–10074 (2009) PMID:19702288 [View Article](#) [PubMed/NCBI](#)
77. Zhurko, G.A., Zhurko, D.A.: Chemcraft program Revision 1.6. Grigoriy A. Zhurko, United States (2012). [View Article](#)